Photodecomposition of Organic Peroxides Containing Coumarin Chromophore: Spectroscopic Studies

Dmitry E. Polyansky and Douglas C. Neckers*

Center for Photochemical Sciences,[1] Bowling Green State University, Bowling Green, Ohio 43403

Received: November 30, 2004; In Final Form: January 26, 2005

The photodecomposition of coumarin-3-*t*-Bu peroxyester (**1**) and coumarin-3-carbonyl-*m*-chlorobenzoylperoxide (**2**) has been studied using nanosecond and femtosecond spectroscopy to elucidate the nature of transient species involved. Excitation of the coumarin chromophore leads to its singlet excited-state decaying with the rate 9×10^9 s^{-1} that results from a composite of emission, intersystem crossing, thermal relaxation, and −O−O− bond homolysis. Dissociation of the weak oxygen−oxygen bond proceeds from both triplet and singlet excited states. The nature of this combination of states is predissociative rather than dissociative as demonstrated by the relatively slow rates of oxygen−oxygen bond rupture. The decomposition of **1** and **2** leads to the formation of coumarin-3-carbonyloxyl radical (**R1**). The later was observed spectroscopically on the nanosecond time scale using both time-resolved FTIR and UV−vis transient techniques. **R1** is consumed in two competitive processes: unimolecular decarboxylation and bi-molecular hydrogen atom transfer. The rates of these reactions are 4.3×10^5 s^{-1} and 1×10^6 M^{-1} s^{-1} respectively. The transition state geometries and energies of decarboxylation of **R1** have been determined using DFT calculations and are compared with values for the benzoyloxyl radical. The decarboxylation of **R1** proceeds via a transition state in which the carboxyl group is almost perpendicular (dihedral angle 114°) to the plane of the coumarin chromophore. The transition state of the benzoyloxyl radical, in contrast, is flat (0°). The varied transition state energies of the radicals (13.6 kcal/mol for coumarin carboxyl radical vs 8 kcal/mol for benzoyloxyl radical) correlate with different decarboxylation rates of these two species.

Introduction

Organic peroxides are widely used to initiate free radical reactions including polymerization.[2−4] The lack of efficient UV−vis absorption of conventional thermal peroxides has led to extensive studies of compounds containing a light absorber and peroxide functionality. Among these are peroxyesters containing benzophenone,[2] naphthalene,[5] anthracene,[6] fluorenone,[7] fluorene,[8] and other chromophores. Despite structural differences, the photodecomposition of peroxyesters follows a common pathway. Excitation leads to rapid cleavage of the oxygen−oxygen bond and formation of the corresponding aroyloxyl radical.[8] Decarboxylation rates of the latter depend mostly on structure and can vary from several picoseconds[8] to tens of microseconds.[9] There are two predominant theories of peroxide photodecomposition. According to the first, decomposition is a concerted process involving simultaneous cleavage of the O−O bond and the $C_{ipso}-C_{carbonyl}$ bond leading to the instantaneous evolution of carbon dioxide.[10] However, recent spectroscopic studies have shown that photodecomposition can also be stepwise in which decarboxylation follows the O−O bond cleavage. In some instances, vibrationally excited states of the aroyloxyl radicals are formed resulting in ultrafast decarboxylation kinetics and preventing one from clearly distinguishing the two mechanisms.[11]

In the current work, we have designed new peroxide systems containing an efficient light absorbing coumarin chromophore. The presence of the carbonyl group in the coumarin moiety allows direct observation of the coumarin-3-carbonyloxyl radical by time-resolved infrared spectroscopy. To the best of our knowledge, this is the first direct observation of an aroyloxyl radical by TRIR.[12] Nanosecond and femtosecond spectroscopic studies as well as product analysis have been carried out to elucidate the nature of transient species involved in the decomposition mechanism.

Experimental Section

General. ^1H and NMR spectra were recorded on Bruker Avance 300 MHz system, and ^{13}C NMR spectra were obtained with Varian Unity+ 400 MHz instrument. GC-MS and DIP mass spectra were measured on Shimadzu GC/MS-QP5050A spectrometer. HPLC measurements were performed on Hitachi LC-7000 series instrument equipped with Alltech Nucleosil C18 column. UV−vis spectra were measured with Shimadzu UV-2401PC spectrophotometer. Steady-state photoluminescence spectra were recorded on Jobin-Yvon Fluorolog-3 FL-11 spectrofluorimeter (450 W Xe lamp, R928 Hamamatsu single photon counting PMT detector). Photodecomposition quantum yields were obtained by direct irradiation of samples with OmNichrome Series 74XA HeCd laser (325 nm) interrupted with Uniblitz SD-10 shutter drive timer. IR-ATR spectra of solid samples were measured on Thermo Nicolet IR200 ATR equipped spectrometer.

Materials. Coumarin-3-carboxylic acid was purchased from Aldrich (99%) and used as received. Coumarin-3-*t*-Bu-peroxyester and coumarin-3-carbonyl chloride were prepared from coumarin-3-carboxylic acid, purified and characterized as described in the Supporting Information. All spectroscopic samples were thoroughly dried, and the purity was verified by HPLC.

* To whom correspondence should be addressed. E-mail: neckers@photo.bgsu.edu.

10.1021/jp044554q CCC: $30.25
Published on Web 03/04/2005

SCHEME 1: Structures of Coumarin-3-*t*-Bu-peroxyester (1), Coumarin-3-carbonyl-*m*-chlorobenzoyl Peroxide (2), Coumarin-3-carboxylic Acid (3), Coumarin-3-carbonyloxyl Radical (R1), and Benzoyloxyl Radical (R4)

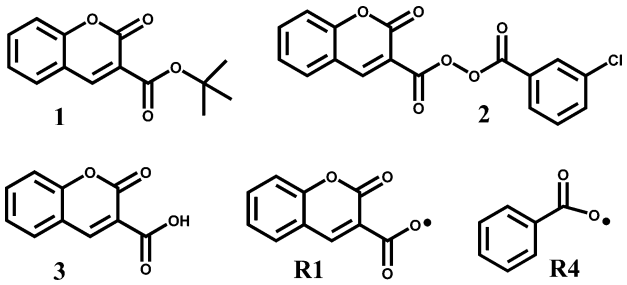

All solvents either for reactions or spectroscopic measurements were dried via distillation over an appropriate drying agent according to standard procedures.[13]

The chemical structures of compounds and intermediates discussed below are shown in Scheme 1.

Nanosecond Infrared Time-Resolved Experiments. Time-resolved FTIR setup has been described elsewhere.[14] Briefly, the third harmonic of a Spectra Physics YAG:Nd^{3+} laser (354.7 nm) was used as an excitation source in all experiments. The laser was operated in pulsed mode with a repetition rate of 10 Hz, and the energy was varied from 1.5 to 5 mJ per pulse. The sample solutions were pumped through a 1 mm thick CaF_2 flow cell with a flow rate up to 150 mL/min. All spectra were recorded in a 1500−2800 cm^{-1} spectral window with a resolution of 8 cm^{-1} every 20 ns. The raw data were processed and visualized with custom written LabView based software.

Nanosecond UV−Vis Time-Resolved Experiments. The detailed description of the time-resolved UV−vis spectrometer is available elsewhere.[15] Briefly, the third harmonic of a Continuum YAG:Nd^{3+} laser (354.7 nm) was used as an excitation source in all experiments. The laser was operated with a repetition rate of 5 Hz, and the energy was kept between 0.5 and 3 mJ per pulse. Solutions were pumped through a quartz flow cell with three polished windows with flow rate up to 150 mL/min. Transient UV−vis spectra were acquired every 10 nm in the 330−820 nm spectral interval.

Femtosecond UV−Vis Time-Resolved Experiments. A detailed description of the home-built ultrafast UV−vis setup is available elsewhere.[16] Briefly, the frequency converted (340 nm) output from a Spectra-Physics Hurricane femtosecond laser was used as an excitation source. The probe pulses were generated in CaF_2 crystal and overlapped with the pump inside the sample flow cell. The solution was degassed with Ar to avoid the formation of long living intermediates (over 1 ms) and pumped through a 2 mm thick CaF_2 flow cell with a flow rate up to 150 mL/min. The absorption of the sample at excitation wavelength was 0.8−1.0 (2 mm cell) and was constantly checked to ensure the decomposition of the starting material less than 10%.

DFT Calculations. DFT calculations were done using the Gaussian 98 package.[17] The optimized structures and frequencies have been visualized with Molekel software.[18] The geometries were optimized using the B3LYP level of theory with the 6-31+G(d,p) basis set. IR frequencies were calculated on optimized structures using the same basis set. All frequencies reported were scaled up by a factor of 0.96, which is traditionally used for this size of the basis set in DFT calculations.[19] The transition state geometries were calculated with UB3LYP/6-31+G(d,p), and energies were corrected to zero-point vibration effects. For transition states, one imaginary vibrational frequency was observed pertinent to the decarboxylation reaction coordinate. Finally, the potential energy along the reaction path in the neighborhood of the transition state was calculated requesting IRQ keyword in Gaussian 98. The maximum of the potential energy was observed at the transition state decreasing along the reaction coordinate.

TABLE 1: Photodecomposition Products of 3-coumarin-*t*-Bu Peroxyester in Different Solvents

solvent	concentration, mM	photoproducts [a]
CCl_4	1.0	3-chlorocoumarin (100%)
CCl_4	10.0	3-chlorocoumarin (52%), 3-coumarin carboxylic acid (35%), coumarin (13%)
CH_3CN	1.0	3-coumarin carboxylic acid (31%), coumarin (69%)
CD_3CN	1.0	3-coumarin carboxylic acid (31%), coumarin (69%)

[a] HPLC yields are shown in parentheses.

Results

Steady-State Studies. Irradiation of coumarin-3-*t*-Bu-peroxyester (**1**) in non-chlorinated solvents (e.g., acetonitrile) at 350 nm yields coumarin, *t*-Bu alcohol, acetone, and coumarin-3-carboxylic acid as the major photochemical products as observed by NMR and IR spectroscopy. In chlorinated solvents (chloroform, dichloromethane, and carbon tetrachloride) formation of 3-chlorocoumarin and a complete or partial disappearance of coumarin are the main differences. Product distribution does not depend on substitution of hydrogen-containing solvents with their deuterated analogues, which indicates no isotopic effect on the hydrogen atom transfer from solvent to the coumarin carbonyloxyl radical (Table 1). Remarkably, even in carbon tetrachloride at concentrations equal to or higher than 10 mM, a substantial amount of coumarin-3-carboxylic acid was observed, whereas at concentrations about 1 mM, 3-chlorocoumarin was the only photochemical product detected (Table 1).

Irradiation of a 1 mM solution of coumarin-3-carbonyl-*m*-chlorobenzoylperoxide (**2**) in carbon tetrachloride yielded 3-chlorocoumarin as the only photochemical product. Due to the limited solubility of **2** in CCl_4 (1mM maximum), concentration dependence studies could not be performed for this compound. The irradiation of **2** in acetonitrile gives photoproducts similar to those formed from **1**.

The quantum yields of photodecomposition of **1** ($\Phi = 0.67$) and **2** ($\Phi = 0.70$) were measured in acetonitrile by irradiating optically concentrated (OD > 10) solutions in a 1 cm quartz cell using the defocused output from a HeCd laser (325 nm). Decomposition was followed by HPLC using biphenyl as the internal standard.

Steady-state photoluminescence spectra of coumarin-3-carboxylic acid (**3**) were measured in degassed acetonitrile solutions in the spectral range from 360 to 600 nm upon excitation at 350 nm. The emission maximum was observed at 425 nm, and its intensity was slightly decreased upon purging with oxygen. The fluorescence quantum yield for **3** ($\Phi_{fl} = 0.03 \pm 0.002$) was measured in acetonitrile using 9-bromoanthracene as a standard.[20] We were not able to obtain accurate Φ_{fl} values for **1** due to its decomposition under the experimental conditions. However, an estimated fluorescence quantum yield of **1** in acetonitrile is about 2.5 times lower than that of **3**.

Nanosecond Time-Resolved FTIR and UV−Vis Studies. Transient FTIR spectra of **1** taken between 700 ns and 2.5 μs after the laser flash are shown in Figure 1. The formation of

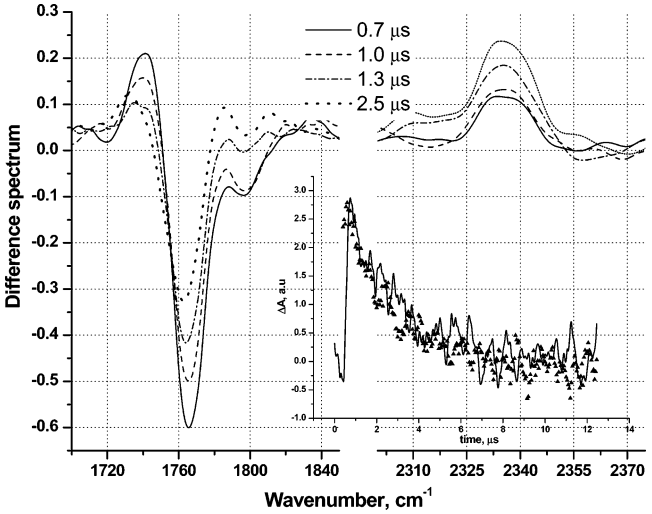

Figure 1. FTIR difference spectra of **1** in CCl_4 acquired between 0.7 μs and 2.5 μs after the laser pulse. The inset shows an overlay of the 1740 cm^{-1} transient decay (solid line) and inverted 2335 cm^{-1} (triangles) growth.

the negative absorbance signals at 1765 cm^{-1} and 1795 cm^{-1} corresponding to the ground-state decay and positive transient corresponding to transient absorption at 1740 cm^{-1} were observed "instantaneously" (within the response time of the instrument) after the laser pulse. Bleaching of the ground state absorption had partially recovered after the first 5 μs and then remained unchanged until the end of the acquisition time ca. 500 μs.

The decomposition of peroxides at room temperature is an irreversible process and the recovery of some ground state bleaching in our case is due to the formation of photostationary products, which in the case of carbon tetrachloride as a solvent was mostly 3-chlorocoumarin (1757 cm^{-1}): the product of chlorine atom transfer from the solvent to the coumarin carbon-centered radical. We did not observe any transient signals which might possibly be associated with a coumarin carbon-centered radical. The DFT calculations show that the frequency of the carbonyl stretching band for these species should be around 1765 cm^{-1}. The absence of any transient evidence for this radical is probably due to overlapping absorptions of the starting material, the 3-coumarin carbon centered radical, and 3-chlorocoumarin.

The transient at 1740 cm^{-1} decayed concomitantly with the rise of the characteristic band at 2335 cm^{-1} (Figure 1, inset). This transient was formed within the first 5 μs, and its amplitude remained unchanged until the end of the acquisition. The strong absorption at 2335 cm^{-1} was observed in the steady state IR spectra of UV-irradiated peroxide solutions. The degassing of irradiated solutions with argon for 10 min totally eliminated the absorption at 2335 cm^{-1}. Thus, the 2335 cm^{-1} band can be unambiguously assigned to the absorption of carbon dioxide.

The kinetic data show that the 1740 cm^{-1} transient is a direct precursor of carbon dioxide. This is the first strong argument for the assignment of this transient to the coumarin-3-carbonyloxyl radical (**R1**). Saturation of the peroxide solutions with oxygen did not decrease the lifetime of the 1740 cm^{-1} band; however, the addition of 20 mM of acrylonitrile totally eliminated the observed transient. The sensitivity of the observed species to acrylonitrile, a known radical scavenger, indicates their radical nature, but the low reactivity toward oxygen points to the oxygen centered radical.[21,22]

The table below summarizes vibrational frequency values of **R1** measured in different solvents and its calculated value in a vacuum. Calculations show excellent agreement with experiment data and follow the trend of decreasing the vibrational frequency of the carbonyl group with increasing solvent polarity.

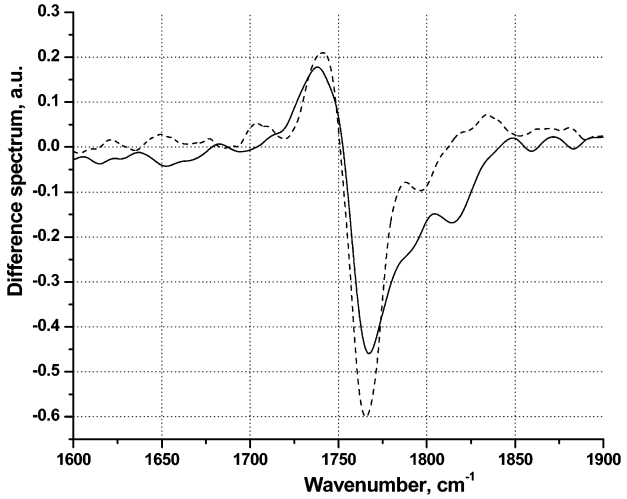

Figure 2. FTIR spectra of **1** (dashed line) and **2** (solid line) taken 1 μs after the laser pulse.

vibrational frequency, cm^{-1}	solvent system
1744	vacuum (calculated)
1740	CCl_4
1727	$CHCl_3$
1720	CH_3CN

Steady-state studies show that at higher concentrations intermolecular hydrogen atom transfer to **R1** from the *tert*-butyl groups of the starting material takes place. In that one might expect decarboxylation to compete with the hydrogen atom transfer, we synthesized the coumarin peroxyester **2** which has no labile hydrogen atoms to obtain an accurate value of the decarboxylation rate of **R1**.

The photochemistry of **2** is essentially the same as that of **1**. The transient infrared spectrum of **2** contains a band at 1740 cm^{-1} that was previously assigned to **R1** (Figure 2).

An interesting feature of the transient behavior of **2** compared to **1** is the biexponential growth of the signal corresponding to the formation of carbon dioxide (Figure 3). The first fast component of this kinetic trace with the lifetime 160 $\pm$ 20 ns corresponds to the decarboxylation of the 3-chlorobenzoyloxyl radical. The decarboxylation rate of this radical as reported by Ingold et al.[22] using time-resolved UV−vis spectroscopy was 5.5 $\times$ 10^6 s^{-1} ($\approx$ 180 ns), which shows good agreement with our data. The lifetime of the second component was 2.8 $\pm$ 0.4 μs, whereas the lifetime of the decay of the 1740 cm^{-1} transient was 3.3 $\pm$ 0.3 μs. Apparently, the second, longer component of carbon dioxide formation is due to the decarboxylation of **R1**.

We have obtained the transient UV−vis spectra from photolysis of **1** and **2** in argon-saturated carbon tetrachloride (Figure 4). The transient UV−vis spectra of aroyloxyl radicals have characteristic broad absorption in the visible and infrared regions of the spectrum.[5,9,21,22] Both spectra show two spectral features: one band around 400 nm and another broad band with a maximum at $\approx$800 nm. Evidently, both spectra originate from the same transient species as can be seen from the similarity in their shape and positions of maxima. The transients observed in our UV−vis experiments are like those assigned in previous studies to aroyloxyl radicals.

Convincing evidence for assignment of the broad band in the visible region of the spectrum to the **R1** radical would come

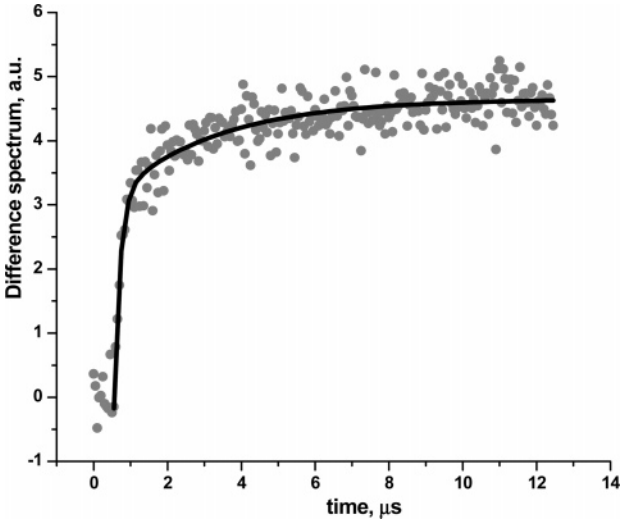

Figure 3. Growth of 2335 cm^{-1} transient after the irradiation of **2** with a 355 nm laser pulse. The dots represent the experimental data points, and the solid line is the biexponential fit (160 ns and 2.8 μs).

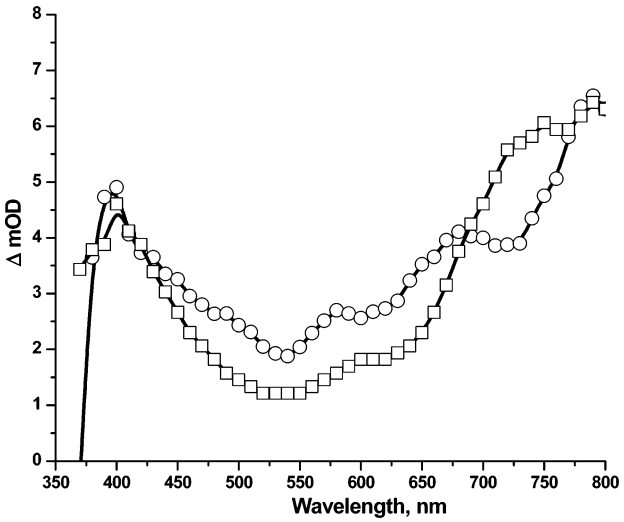

Figure 4. Normalized transient UV−vis spectra of **1** (circles) and **2** (squares) measured 200 ns after laser pulse.

from direct comparison of the lifetime of the radical measured in time-resolved IR experiments with lifetimes obtained using transient UV−vis spectroscopy. The absorption at 770 nm was chosen to monitor the kinetics of the decarboxylation process. The kinetic studies indicate a strong dependence of the observed lifetimes in both IR and UV−vis experiments upon excitation energy. At laser energies higher than 1.5 mJ/pulse, the observed lifetimes decreased with an increase in the laser energy, and at energies over 8 mJ/pulse, the kinetic traces reveal multicomponent character. We were only able to match lifetimes obtained in the TRIR experiment (2.6 ± 0.3 μs) and TR UV−vis measurements (2.3 ± 0.1 μs) at energies lower than 1.5 mJ/pulse. The similar lifetimes of the 1740 cm^{-1} transient and the decay rate of the broad VIS−NIR absorption allow the assignment of these two transient spectra obtained by different spectroscopic techniques to the same species, namely, the coumarin-3-carbonyloxyl radical.

UV−vis transient spectroscopy was used to study the decomposition kinetics of **R1**. The dispersive technique used to acquire spectral information in the transient UV−vis setup allowed us to use a single wavelength to monitor individual kinetic traces as opposed to FTIR setup that collects complete

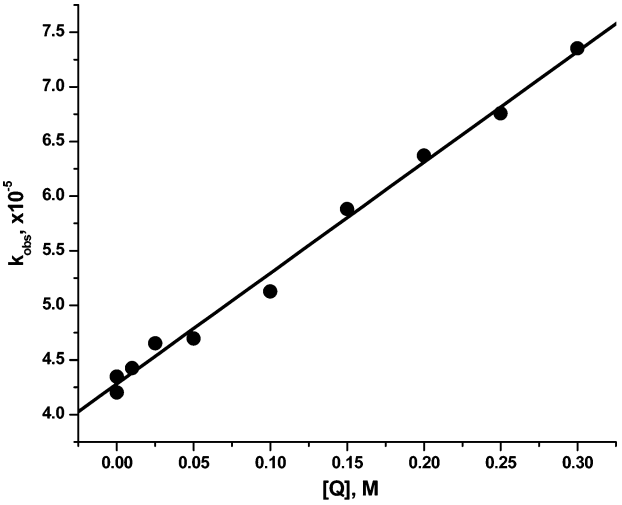

Figure 5. Stern-Volmer plot of the quenching of coumarin-3-carbonylxyl radical by di-*t*-Bu-peroxide.

spectral information in a single experiment. The first approach appeared to be faster and required less sample.

Based on these steady state and transient spectroscopy studies, there are two major channels leading to the disappearance of **R1**: intramolecular decarboxylation and intermolecular hydrogen atom transfer. Since the concentration of the products at the early stages of irradiation is negligible compared to **1**, we assume that the source of the hydrogen atoms in the bi-molecular reaction should be the *tert*-butyl groups of the starting material. This suggested the use of di-*tert*-butylperoxide as a quencher in kinetic experiments assuming that the chemical environment of hydrogen atoms in the *tert*-butyl group is close to the hydrogen−carbon bond energy of the starting peroxide. Di-*tert*-butylperoxide cannot participate in primary photochemical reactions due to the lack of absorption at 355 nm, and it plays the role solely of hydrogen atom donor. Due to their insignificant absorption in this spectral region, the possible products formed from this quencher should also not interfere with the signal at 770 nm.[23] A Stern−Volmer plot of the quenching of **R1** with di-*tert*-butylperoxide is shown in Figure 5. The value of bimolecular rate determined from the slope was (1.01±0.02)-10^6 $M^{-1}s^{-1}$ and the rate of decarboxylation reaction found as the intercept was (4.28±0.04)10^5 s^{-1}.

Ultrafast Measurements. UV−vis transient spectra of **1** and **3** in acetonitrile were obtained with picosecond time resolution. Excitation of the coumarin chromophore with a 340 nm laser pulse leads to the "instantaneous" (within the pulse width) formation of a broad absorption between 450 and 700 nm with the maximum around 550 nm (Figure 6) observed for **1** as well as for **3**. The similar spectral features observed for each compound indicates that the transient at 550 nm originates from an excited state rather from the chemically produced transient species since the model compound **3** does not possess substantial reactivity under experimental conditions.

For **3** the rate of the decay of the 550 nm transient was 5 × 10^9 s^{-1} which is a composite resulting from emission, intersystem crossing, and thermal relaxation (Table 2). This decay is accompanied by the growth of an absorption around 375 nm with a rate[24] 3.3 × 10^9 s^{-1} (Figure 7). The same band was observed decaying with a rate of ∼10^5 s^{-1} as measured using nanosecond transient UV−vis experiment (Figure 8). The sensitivity of this transient to oxygen and the similarity of its spectroscopic features to those reported previously[25] allow us to assign this absorption to the triplet excited state of the coumarin-3-carboxylic acid. We assign the 550 nm transient to

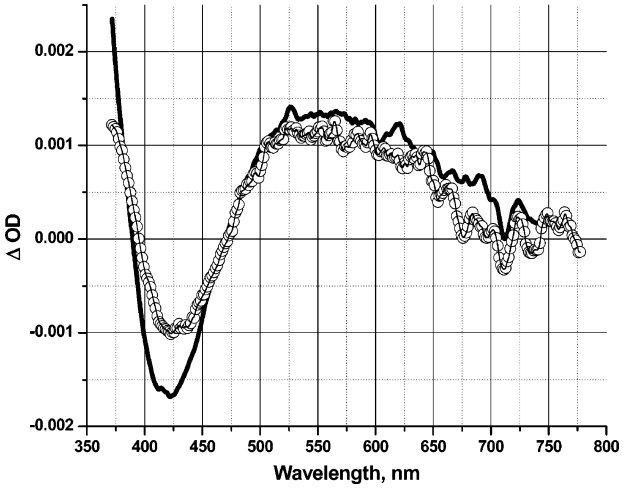

Figure 6. Normalized transient UV−vis spectra of **1** (circles) and **3** (solid) measured 10 ps after the 340 nm femtosecond laser pulse.

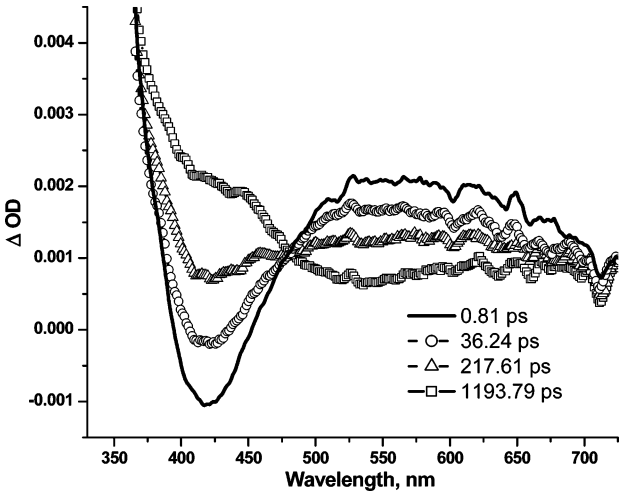

Figure 7. Transient UV−vis spectral evolution of **3** after the 340 fs laser pulse.

TABLE 2: Decay Rates of Transient Species Observed for 1 and 3, Fluorescence Quantum Yield of 3, and Photodecomposition Quantum Yield of 1

compound	550 nm decay, s^{-1}	375 nm growth, s^{-1}	375 nm decay, s^{-1}	Φ_{FL}	Φ_{O-O} (Ar)	Φ_{O-O} (O_2)
1	9×10^9				0.67	0.56
3	5×10^9	3.3×10^9	$\sim 10^5$	0.03		

the singlet exited state absorption of the coumarin chromophore based on the fact that this transient is the direct precursor of the 375 nm absorption assigned previously to the T_1-T_n transition.

The presence of the peroxide functionality decreases the lifetime of the 550 nm transient about two times which corresponds to the rate 9×10^9 s^{-1}. The difference in rates between **1** and **3** could be used to calculate the rate (k_{O-O}) and quantum yield ($\Phi_{O-O}{}^S$) of peroxide bond scission from the singlet excited state (Table 3).

Ab Initio Calculations of Decarboxylation Thermodynamics. A direct comparison of reactivity of benzoyloxyl radical (**R4**) and coumarin-3-carbonyloxyl radical (**R1**) has been performed by calculating the transition state energies of the decarboxylation reaction (UB3LYP/6-31+G**). The ground-state geometries of **R1** and **R4** are planar, with carboxyl groups laying in the plane of the benzene or coumarin ring (Figure 9). The transition state of **R4** is also planar with the C−CO_2 bond

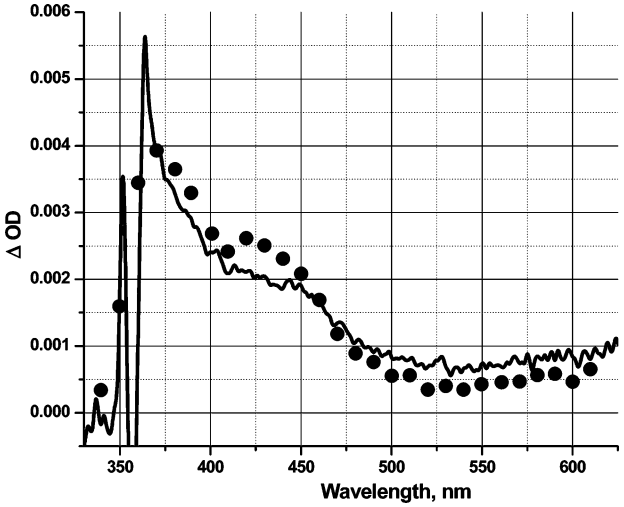

Figure 8. Normalized transient UV−vis spectra of **3** taken 10 ps (solid) and **2** μs (dot) after the laser pulse.

TABLE 3: Rates and Efficiencies of Photophysical and Photochemical Pathways Measured for 1 and 3

compound	k_{FL}, $s^{-1}x10^{-9}$	k_{ISC}, $s^{-1}x10^{-9}$	k_{NR}, $s^{-1}x10^{-9}$	k_{O-O}, $s^{-1}x10^{-9}$	Φ_{ISC}	$\Phi_{O-O}{}^S$
1	0.15	3.3	1.55	4.0	0.37	0.44
3	0.15	3.3	1.55		0.37	

elongated from 1.473 to 1.958 Å. The barrier height (ΔE_T) of the decarboxylation reaction of **R4** calculated as a difference between ZPE corrected energies of the **R4** and corresponding transition state (**TS4**) was 8 kcal/mol. The geometry and ΔE_T obtained for **R4** agrees well with previously reported values.[26] In contrast to **R4**, the transition state geometry of **R1** is not planar but has an angle between the plane of coumarin chromophore and carboxyl group about 66° and the C−CO_2 distance 1.974 Å (Figure 9). The ΔE_T of the decarboxylation reaction of **R1** calculated as a difference between ZPE corrected energies of the **R1** and corresponding transition state (**TS1**) was 13.6 kcal/mol. The graph of potential energy surface along reaction coordinate corresponding to decarboxylation of **R1** (Figures S1 and S2) and computational details can be found in Supporting Information.

Discussion

Compounds containing the coumarin chromophore are well-known laser dyes and possess high fluorescence quantum yields. However, the photophysical properties of coumarin systems greatly depend on their electronic structure.[27,28,29] As opposed to 7-substituted coumarins, coumarin-3-carboxylic acid and corresponding esters have low fluorescence quantum yields due to radiationless deactivation of the singlet excited state as determined by steady-state experiments.[28,29] Our ultrafast measurements show that intersystem crossing and vibrational relaxation are the dominant routes of singlet excited-state decay. Nevertheless, the introduction of the carboxyl group into the coumarin chromophore decreases the intersystem crossing rate and increases the fluorescence quantum yield compared to coumarin itself.[29] The triplet excited state formed has an appreciably long lifetime ($\sim$10 μs) and decays predominantly via vibrational relaxation and bimolecular quenching processes.

The comparison of the intersystem crossing rate and the rate of oxygen−oxygen bond cleavage indicates that the peroxide decomposition proceeds mostly from the singlet excited state of the coumarin chromophore. However, the photodecomposi-

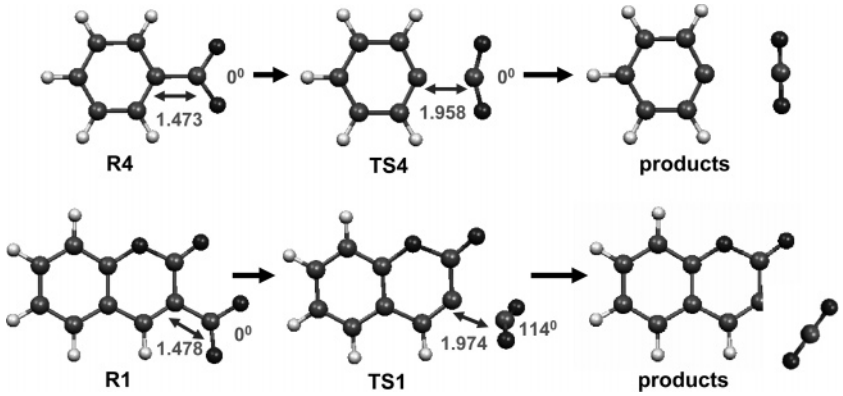

Figure 9. Calculated (UB3LYP/6-31+G**) geometries of **R1** (bottom) and **R4** (top) and their transition states (**TS1** and **TS4**) of decarboxylation process. The dihedral angles between plane of the chromophore and CO_2 group are shown next to each structure.

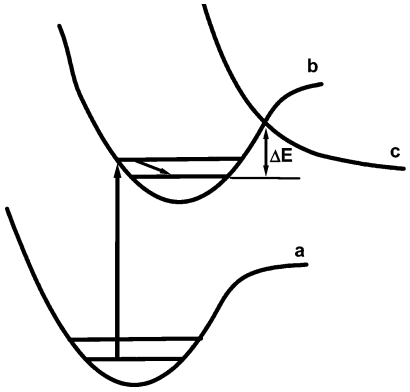

Figure 10. Schematic representation of photochemical reaction from predissociative excited state. Legend: a, ground state; b, electronically excited bound state; c, dissociative state; Δ*E*, barrier of crossing from b to c.

tion quantum yield (Φ^{S}_{O-O}) derived from the rates obtained from kinetic measurements was about 30% lower than the photodecomposition quantum yield measured directly (see Table 2 and Table 3) which points to the substantial contribution of the triplet state into overall peroxyester decomposition. The triplet excited state formed possesses sufficient energy[30−32] to provide efficient cleavage of the oxygen−oxygen peroxide bond[33] therefore providing another precursor for the peroxide photodecomposition process. Consequently, the cleavage of the O−O bond proceeds from the singlet as well as from the triplet excited states with contributions of 66% and 34% respectively. The sensitivity of the peroxyester photodecomposition quantum yield to oxygen (Table 2) provides additional supporting evidence for participation of the triplet state in the photochemical reaction. As has been shown previously in studies of the photosensitized decomposition of hydrogen peroxide, a series of singlet and triplet excited states are adiabatically correlated with ground states of hydroxyl radicals, and both singlet and triplet sensitized decomposition of peroxide is possible.[34]

Unfortunately, direct observation of the triplet state kinetics in **1** was not possible due to instrumental limitations;[35] however, taking into account the slow rates ($\sim 10^5$ s^{-1}) of triplet disappearance obtained for **3** and the lack of spectroscopic evidence for the presence of the triplet state in **1** on a nanosecond time scale, we assume that all of the triplet state population is consumed by chemical reaction. This suggests that the quantum yield of peroxide photodecomposition from the triplet excited state equals the quantum efficiency of the triplet state production. However, the sum of photodecomposition quantum yields from triplet and singlet states is higher than the quantum yield measured directly which we believe is due to overestimation of the intersystem crossing rate constant and therefore the quantum efficiency of the triplet state formation.

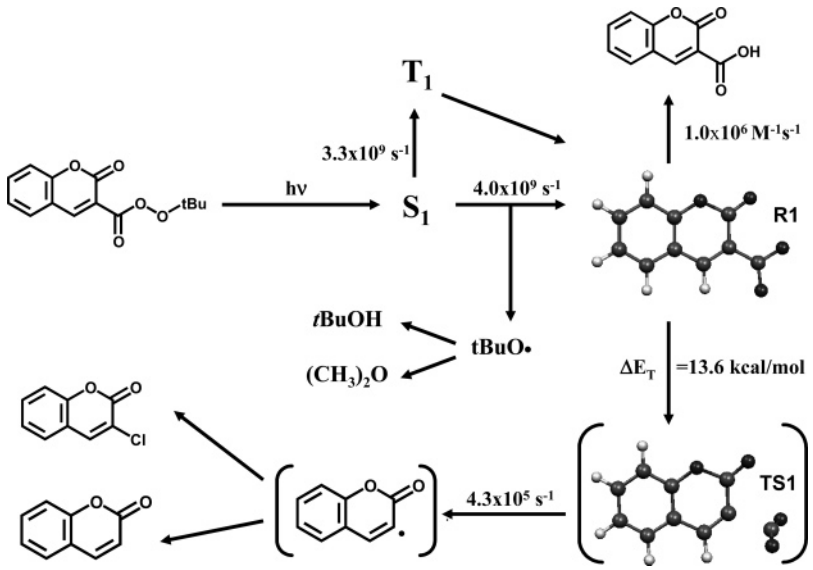

Figure 11. General photodecomposition scheme of **1**. Species in parentheses are suggested (calculated) structures. The measured rates of chemical and photophysical processes are indicated above corresponding arrows.

The magnitude of the rate of O−O dissociation provides insight into the nature of the potential energy surface. It is known that dissociative surfaces are barrierless and the promotion of a molecule directly into a dissociative state leads to a very rapid (≈ hundreds of femtoseconds) dissociation.[36−39] In the case of **1**, the rate of the O−O bond rupture is 250 ps, which is about 10^3 times longer than for dissociative states. Even though we were not able to measure triplet state decay directly, the sensitivity of the photodecomposition quantum yield to oxygen indicates that at least a part of the triplet state is quenched in a bimolecular process. Assuming triplet quenching to be diffusion limited, the rate of O−O bond cleavage should be on the order of nanoseconds which also argues against the repulsive nature of the triplet state. Ruling out the dissociative nature of the excited states, we propose peroxide decomposition proceeds according to an electronic predissociation process.[38,40] In this case, molecules are promoted into bound excited states that do not themselves dissociate but can cross into dissociative surfaces. There is a certain barrier for this chemical process that depends on coupling between two states, and this barrier determines the rate of the dissociation (Figure 10).

The monoexponential character of the decay of **R1** and the formation of CO_2 indicates that decarboxylation of **R1** proceeds from vibrationally excited ground state only. This is in contrast to the situation reported with a series of aroyloxyl radicals, which have been shown to undergo decarboxylation from both vibronically excited and ground states.[11,26] We believe that in our case the excess of vibrational energy dissipates before radicals are formed due to slower O−O bond scission.

The decarboxylation rate of **R1** was about an order of magnitude lower than the rate of decarboxylation of either the benzoyloxyl radical or the 2-naphthyloxyl radical. DFT calculations of the transition states agree with this experimental observation. The decarboxylation barrier for radical **R1** is 5.6 kcal/mol higher than for **R4**, implying slower decarboxylation rates of **R1** compared to **R4**. We attribute this to the stabilization of **R1** by an electron-reach coumarin aromatic system and to the geometrical specifics of the transition state. As proposed by Ingold et al.[22] stabilization of various aroyloxyl radicals via substitution on the aromatic ring is due to conjugative electron delocalization or hyperconjugation between the substituent and the radical site.

Conclusions

The decomposition of coumarin perester proceeds from both triplet and singlet excited states (Figure 11). The nature of this state is predissociative rather than dissociative as demonstrated by the relatively slow rates of oxygen−oxygen bond rupture. The decomposition of **1** and **2** is clearly a stepwise process since the cleavage of O−O bond and the decarboxylation of **R1** can be observed separately on different time scales. **R1** is consumed in two competitive processes − unimolecular decarboxylation and bimolecular hydrogen atom transfer. The rates of these reactions are $4.3 \times 10^5\ s^{-1}$ and $1 \times 10^6\ M^{-1}\ s^{-1}$ respectively. The decarboxylation of **R1** proceeds from vibronically relaxed ground state as can be seen from relatively slow monoexponential kinetics of **R1** decay and CO_2 formation.

Acknowledgment. Authors thank Dr. Evgeny Danilov for assistance with transient spectroscopy and continuous fruitful discussions. The Ohio Laboratory for Kinetic Spectrometry (M. A. J. Rodgers, Dir.) is gratefully acknowledged for providing equipment for transient spectroscopy measurements. One of the authors (D.E.P.) is grateful to the McMaster Endowment for support in the form of a Fellowship.

Supporting Information Available: Synthesis and characterization of compounds **1** and **2**. The Cartesian coordinates of optimized geometries of **R1** and **R4** and corresponding transition states together with their energies and vibrational frequencies. This material is available free of charge via the Internet at http://pubs.acs.org.

References and Notes

(1) Center for Photochemical Sciences Contribution #548.
(2) Neckers, D. C.; Abu-Abdoun, I. *Macromolecules* **1984**, *17*, 2468−2473.
(3) Neckers, D. C. Photopolymerizable Composition Containing Perester Photoinitiator and Photopolymerization Process. U.S. Patent 4,498,-963, 1985.
(4) Neckers, D. C. Method for Polymerizing a Bis(Allyl Carbonate). U.S. Patent 4,561,951, 1985.
(5) Najiwara, T.; Hashimoto, J.; Segawa, K.; Sakuragi, H. *Bull. Chem. Soc. Jpn.* **2003**, *76*, 575−585.
(6) Rapaport, E.; Cass, M. W.; White, E. H. *J. Am. Chem. Soc.* **1972**, *94*, 3160−3167.
(7) Humphreys, R. W. R. Visible Light Absorbing Peroxy-Esters. U.S. Patent 4,604,295, 1986.
(8) Falvey, D. E.; Schuster, G. B. *J. Am. Chem. Soc.* **1986**, *108*, 7419−7420.
(9) Wang, J.; Itoh, H.; Tsuchiga, M.; Tokumaru, K.; Sakuragi, H. *Tetrahedron* **1995**, *51*, 11967−11977.
(10) Bartlett, P. D.; Hiatt, R. R. *J. Am. Chem. Soc.* **1958**, *80*, 1398−1405.
(11) Abel, B.; Buback, M.; Kling, M.; Schmatz, S.; Schroeder, J. *J. Am. Chem. Soc.* **2003**, *125*, 13274−13278.
(12) The time-resolved IR spectroscopy in the region from 3 to 5.1 μm was used to observe aroyloxy radicals indirectly by monitoring the CO_2 release. For example, see: Buback, M.; Kling, M.; Schmatz, S.; Schroeder, J. *Phys. Chem. Chem. Phys.* **2004**, *6*, 5441−5455.
(13) Perrin, D. D.; Armarego, W. L. F. *Purification of Laboratory Chemicals*; Butterworth Heinemann: Oxford, U.K., 1994.
(14) Fedorov, A. V.; Danilov, E. O.; Merzlikine, A. G.; Rodgers, M. A. J.; Neckers, D. C. *J. Phys. Chem. A* **2003**, *107*, 3208−3214.
(15) Merzlikine, A. G.; Voskresensky, S. V.; Danilov, E. O.; Fedorov, A. V.; Rodgers, M. A. J.; Neckers, D. C. *Photochem. Photobiol. Sci.* **2004**, *3*, 892−997.
(16) Gentili, P. L.; Danilov, E.; Ortica, F.; Rodgers, M. A. J.; Favaro, G. *Photochem. Photobiol. Sci.* **2004**, *3*, 886−891.
(17) Frisch, M. J.; Trucks, G. W.; Schlegel, H. B.; Scuseria, G. E.; Robb, M. A.; Cheeseman, J. R.; Zakrzewski, V. G.; Montgomery, J. A., Jr.; Stratmann, R. E.; Burant, J. C.; Dapprich, S.; Millam, J. M.; Daniels, A. D.; Kudin, K. N.; Strain, M. C.; Farkas, O.; Tomasi, J.; Barone, V.; Cossi, M.; Cammi, R.; Mennucci, B.; Pomelli, C.; Adamo, C.; Clifford, S.; Ochterski, J.; Petersson, G. A.; Ayala, P. Y.; Cui, Q.; Morokuma, K.; Malick, D. K.; Rabuck, A. D.; Raghavachari, K.; Foresman, J. B.; Cioslowski, J.; Ortiz, J. V.; Stefanov, B. B.; Liu, G.; Liashenko, A.; Piskorz, P.; Komaromi, I.; Gomperts, R.; Martin, R. L.; Fox, D. J.; Keith, T.; Al-Laham, M. A.; Peng, C. Y.; Nanayakkara, A.; Gonzalez, C.; Challacombe, M.; Gill, P. M. W.; Johnson, B. G.; Chen, W.; Wong, M. W.; Andres, J. L.; Head-Gordon, M.; Replogle, E. S.; Pople, J. A. *Gaussian 98*, revision A.7; Gaussian, Inc.: Pittsburgh, PA, 1998.
(18) *MOLEKEL 4.0*; Flükiger, P.; Lüthi, H. P., Portmann, S.; Weber, J.; Swiss Center for Scientific Computing: Manno, Switzerland, 2000.
(19) Foresman, J. B.; Frisch, A. *Exploring Chemistry with Electronic Structure Methods*; Gaussian: Pittsburgh, PA, 1996.
(20) Melhuish, W. H. *J. Phys. Chem.* **1961**, *65*, 229−235.
(21) Chateauneuf, J.; Lusztyk, J.; Ingold K. U. *J. Am. Chem. Soc.* **1988**, *110*, 2877−2885.
(22) Chateauneuf, J.; Lusztyk, J.; Ingold K. U. *J. Am. Chem. Soc.* **1988**, *110*, 2886−2893.
(23) Avila, D. V.; Ingold, K. U.; Dinardo, A. A.; Zerbetto, F.; Zgierski, M. Z.; Lusztyk, J. *J. Am. Chem. Soc.* **1995**, *117*, 2711−2718.
(24) We should note that the rate of the triplet excited state formation is a good estimate rather than exact value due to multicomponent nature of the 370−500 nm region. The absorption band of the triplet state is partially overlapped with ground-state absorption in its blue part and some of the singlet state absorption in the red part assuming symmetric shape of 550 nm band.
(25) Kawata, H.; Ichikawa, S.; Kumagai, T.; Niizuma, S. *Tetrahedron Lett.* **2002**, *43*, 5161−5163.
(26) Abel, B.; Assmann, J.; Botschwina, P.; Buback, M.; Kling, M.; Oswald, R.; Schmatz, S.; Schroeder, J.; Witte, T. *J. Phys. Chem. A* **2003**, *107*, 5157−5167.
(27) Seixas de Melo, J. S.; Becker, R. S.; Macanita, A. L. *J. Phys. Chem.* **1984**, *98*, 6054−6058.

(28) Azuma, K.; Suzuki, S.; Uchiyama, S.; Kajiro, T.; Santa, S.; Imai, K. *Photochem. Photobiol. Sci.* **2003**, *2*, 443−449.

(29) Mantulin W. W., Song P−S. *J. Am. Chem. Soc.* **1973**, *95*, 5122−5129.

(30) The T_1 energy of ∼60 kcal/mol was estimated from phosphorescence data of **3** reported in refs 29, 31, and 32.

(31) Bello, J.; Hurtubise, R. *J. Appl. Spectrosc.* **1986**, *40*, 790−794.

(32) Li, L. D.; Yang, S. Z. *Anal. Chim. Acta* **1994**, *296*, 99−105.

(33) The oxygen−oxygen bond strength in organic peroxyesters is about 35 kcal/mol. Lide, D. R., *CRC Handbook of Chemistry and Physics*; CRC Press: Boca Raton, FL, **2000**.

(34) Ellis, A. B.; Kaiser, S. W.; Wrighton, M. S. *J. Am. Chem. Soc.* **1976**, *98*, 1637−1639.

(35) The maximum time delay of the current setup is 1.6 ns (see ref 16).

(36) Cheng, P. Y.; Zhong, D.; Zewail, A. H. *Chem. Phys. Lett.* **1995**, *237*, 399−405.

(37) Freitas, J. E.; Hwang, H. J.; El-Sayed, M. A. *J. Phys. Chem.* **1994**, *98*, 3322−3329.

(38) Hwang, H. J.; El-Sayed, M. A. *J. Photochem. Photobiol. A* **1996**, *102*, 13−20.

(39) Schinke, R. *Photodissociation Dynamics*; Cambridge University Press: Cambridge, U.K., 1993.

(40) Liu, Y.-J.; Persson, P.; Lunell, S. *J. Phys. Chem. A* **2004**, *108*, 2339−2345.